[20] C. Zhu and A. Kawamura, "The development of biped robot MARI-3 for fast walking and running," in *Proc. IEEE Conf. Humanoid Robot.*, Genoa, Italy, Dec. 2006, pp. 599–604.
[21] B. Ugurlu and A. Kawamura, "ZMP-based online jumping trajectory generation for a one-legged robot," *IEEE Trans. Ind. Electron.*, vol. 57, no. 5, pp. 1701–1709, May 2010.
[22] B. Ugurlu and A. Kawamura, "Eulerian ZMP resolution based bipedal walking: Discussions on the intrinsic angular momentum rate change about center of mass," in *Proc. IEEE Conf. Robot. Autom.*, Anchorage, AK, May 2010, pp. 4218–4223.
[23] Y. Fujimoto and A. Kawamura, "Simulation of an autonomous biped walking robot including environmental force interaction," *IEEE Robot. Autom. Mag.*, vol. 5, no. 2, pp. 33–42, Jun. 1998.
[24] B. Ugurlu, N. G. Tsagarakis, E. Spyrakos-Papastravridis, and D. G. Caldwell, "Compliant joint modification and real-time dynamic walking implementation on bipedal robot cCub," in *Proc. IEEE Conf. Mechatronics*, Istanbul, Turkey, Apr. 2011, pp. 833–838.
[25] P. Kormushev, B. Ugurlu, S. Calinon, N. G. Tsagarakis, and D. G. Caldwell, "Bipedal walking energy minimization by reinforcement learning with evolving policy parameterization," in *Proc. IEEE Conf. Intell. Robots Syst.*, San Francisco, CA, Sep. 2011, pp. 318–324.
[26] W. H. Press, S. A. Teukolsky, W. T. Vetterling, and B. P. Flannery, *Numerical Recipes in C: The Art of Scientific Computing*, 2nd ed. Cambridge, U.K.: Cambridge Univ. Press, 1992.
[27] Q. Li, A. Takanishi, and I. Kato, "A biped walking robot having a ZMP measurement system using universal force-moment sensors," in *Proc. IEEE Conf. Intell. Robots Syst.*, Tokyo, Japan, 1991, pp. 1568–1573.
[28] K. Ohnishi, M. Shibata, and T. Murakami, "Motion control for advanced mechatronics," *IEEE Trans. Mechatronics*, vol. 1, no. 1, pp. 56–67, Mar. 1996.
[29] B. Ugurlu, T. Hirabayashi, and A. Kawamura, "A unified control frame for stable walking," in *Proc. IEEE Conf. Ind. Electron Control*, Porto, Portugal, Nov. 2009, pp. 4167–4172.
[30] J. Kim, I. Park, and J. Oh, "Experimental realization of dynamic walking of the biped humanoid robot KHR-2 using zero moment point feedback and inertial measurement," *Adv. Robot.*, vol. 20, no. 6, pp. 707–736, 2006.
[31] B.-K. Cho, J.-H. Kim, and J. Oh, "Online balance controllers for a hopping and running humanoid robot," *Adv. Robot.*, vol. 25, no. 9–10, pp. 1209–1225, 2011.
[32] C. Chevallereau, D. Djoudi, and J. W. Grizzle, "Stable bipedal walking with foot rotation through direct regulation of the zero moment point," *IEEE Trans. Robot.*, vol. 24, no. 2, pp. 390–401, Apr. 2008.
[33] H. Asada and J. Slotine, "Position control: Why local schemes work," in *Robot Analysis and Control.*. Hoboken, NJ: Wiley, 1986, Sec. 6.2, pp. 136–139.
[34] S. Kagami, T. Kitagawa, K. Nishiwaki, T. Sugihara, M. Inaba, and H. Inoue, "A fast dynamically equilibrated walking trajectory generation method of humanoid robot," *Auton. Robots*, vol. 12, no. 1, pp. 71–82, 2002.
[35] E. Yoshida, J. P. Laumond, C. Esteves, O. Kanoun, T. Sakaguchi, and K. Yokoi, "Whole-body locomotion, manipulation and reaching for humanoids," *Lecture Notes Comput. Sci.*, vol. 5277, pp. 210–221, 2008.
[36] D. T. Greenwood, *Advanced Dynamics*. Cambridge, U.K.: Cambridge Univ. Press, 2003.

Control and Planning of 3-D Dynamic Walking With Asymptotically Stable Gait Primitives

Robert D. Gregg, Adam K. Tilton, Salvatore Candido, Timothy Bretl, and Mark W. Spong

***Abstract*—In this paper, we present a hierarchical framework that enables motion planning for asymptotically stable 3-D bipedal walking in the same way that planning is already possible for zero moment point walking. This framework is based on the construction of *asymptotically stable gait primitives* for a class of hybrid dynamical systems with impacts. Each primitive corresponds to an asymptotically stable hybrid limit cycle that admits rules *a priori* for sequential composition with other primitives, reducing a high-dimensional feedback motion planning problem into a low-dimensional discrete tree search. As a constructive example, we develop this planning framework for the 3-D compass-gait biped, where each primitive corresponds to walking along an arc of constant curvature for a fixed number of steps. We apply a discrete search algorithm to plan a sequence of these primitives, taking the 3-D biped stably from start to goal in workspaces with obstacles. We finally show how this framework generalizes to more complex models by planning walking paths for an underactuated five-link biped.**

***Index Terms*—Asymptotic stability, legged locomotion, path planning, robot control, switched systems.**

I. Introduction

Passive dynamic walking is characterized by phases of instability where the center of mass engages in pendular falling until ground reaction forces redirect this motion into the next step cycle. This interplay between continuous and discrete dynamics results in repetitive motion that is inherently stable from step to step, i.e., perturbations are asymptotically dissipated over a walking sequence. Many real-world robotic systems, such as RABBIT [1], ERNIE [2], MABEL [3], Gibbot [4], and Parkourbot [5], exhibit these *asymptotically stable* gaits. These robots rely on ballistic momentum and gravitational energy to drive their unactuated degrees of freedom (DOFs), e.g., passive rotation of the support foot [1]–[3], [6], which contributes to their speed and energetic efficiency.

However, asymptotically stable walkers currently lack the same functionality as humanoid robots, e.g., some require downhill slopes for strictly gravity-powered walking, are constrained to the sagittal plane of motion, lack directional control authority, and/or lack redundant joints

Manuscript received March 2, 2012; revised June 19, 2012; accepted July 23, 2012. Date of publication August 13, 2012; date of current version December 3, 2012. This paper was recommended for publication by Associate Editor A. Kheddar and Editor J.-P. Laumond upon evaluation of the reviewers' comments. This work was supported by the National Science Foundation under Grant CMMI-0856368, Grant CMS-0510119, and Grant NSF-0931871.

R. D. Gregg is with the Center for Bionic Medicine, Rehabilitation Institute of Chicago, and the Department of Mechanical Engineering, Northwestern University, Chicago, IL 60611 USA (e-mail: rgregg@ieee.org).

A. K. Tilton is with the Department of Mechanical Science and Engineering, University of Illinois at Urbana-Champaign, Urbana, IL 61801 USA (e-mail: atilton2@illinois.edu).

S. Candido is with the Google, Inc., Mountain View, CA 94043 USA (e-mail: scandido@google.com).

T. Bretl is with the Department of Aerospace Engineering, University of Illinois at Urbana-Champaign, Urbana, IL 61801 USA (e-mail: tbretl@illinois.edu).

M. W. Spong is with the Department of Electrical Engineering, University of Texas at Dallas, Richardson, TX 75080 USA (e-mail: mspong@utdallas.edu).

This paper has supplementary downloadable material available at http://ieeexplore.ieee.org.

Color versions of one or more of the figures in this paper are available online at http://ieeexplore.ieee.org.

Digital Object Identifier 10.1109/TRO.2012.2210484

for manipulation. Hybrid nonlinear dynamics make it difficult to prove stability of a given motion—the robot state cannot be checked at each instant against closed-form balance conditions like zero moment point (ZMP, cf., [7]). For this reason, it has been difficult to extend asymptotically stable approaches, which rely on numerical analysis [8], into motion planning applications.

The goal of this paper is to enable motion planning for asymptotically stable dynamic walking in the same way that planning is already possible for ZMP-based walking. We will do so by constructing a set of asymptotically stable "motion primitives" with safety guarantees that are amenable to established planning methods based on ZMP motion primitives.

Motion primitives prescribe a library of common actions, such as walking and climbing, reducing the high-dimensional kinodynamic planning problem to a discrete sequence of precomputed motions [9], [10]. Instead of using motion primitives that track ZMP-constrained joint trajectories, we will build a set of control systems yielding asymptotically stable walking gaits. For this purpose, we adopt the energy-shaping method of controlled reduction [11], which has previously been used to construct 3-D gaits for both straight-ahead walking and constant-curvature steering [12], [13].

Gaits capable of steering with mild curvature have similarly been produced using hybrid zero dynamics in [6]. This approach elegantly exploits the fact that local asymptotic stability implies local input-to-state stability: There exist bounds on path curvature and initial conditions that guarantee a bounded change in state between impacts. However, it is not clear how to derive the bounds for this form of stability (e.g., the maximum curvature safely allowed from some initial state).

This paper contributes a pair of *a priori* rules that ensure stable sequential composition from a set of asymptotically stable gaits derived from *any* low-level controller. We use switched systems theory to prove these rules, considering the more general case of *locally asymptotically* stable (LAS) systems as opposed to *globally exponentially* stable systems in [14]. This stability result reduces a high-dimensional control and planning problem to a low-dimensional discrete tree search, where paths through the workspace correspond to composite (Lyapunov) funnels that obey the rules admitted by a *small* set of controllers. This differs from the pioneering funneling work [15], in which a workspace is robustified by covering it with regions of attraction from *many* locally stabilizing controllers. We extend our preliminary work [16] by 1) implementing a planning algorithm around our two rules; and 2) considering more complex biped models. Hence, we combine control and planning into one coherent approach—we are unaware of other planning results for asymptotically stable 3-D walking.

We begin by describing the 3-D compass-gait biped in Section II, which we use as a canonical example to construct our planning framework. We formalize the notion of *asymptotically stable gait primitives* and the planning problem admitted by such primitives in Section III. We prove bounds on steering curvature and switching frequency that allow stable composition of gait primitives in Section IV, implying that a walking path composed of these primitives may be stably followed by the robot. We derive a set of primitives and composition rules for the compass-gait biped (using controlled reduction) in Section V. We implement a discrete search algorithm in Section VI to plan open-loop primitive sequences for walking through workspaces with obstacles, which we then extend to an underactuated five-link 3-D biped. We conclude with remarks and future work in Section VII.

II. Bipedal Walking as a Hybrid System

In order to study locomotion with impulsive impacts, we must consider both continuous and discrete dynamics in a hybrid system. Bipedal walking gaits correspond to hybrid limit cycles that are stable from step to step. We now use the canonical example of the compass-gait biped to construct the formalisms necessary for our planning framework.

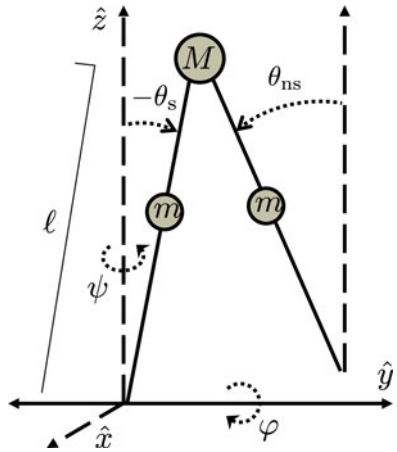

Fig. 1. Three-dimensional extension of the compass-gait biped.

The 3-D extension of the planar compass-gait biped is shown in Fig. 1. The generalized configuration space of this two-link model is $\mathrm{SE}(3) \times \mathbb{S}^1$, where the stance foot has six DOFs (three position and three orientation) and the hip has one rotational DOF. Assuming the ground has sufficient friction and the stance foot is sufficiently large to remain in contact without slipping or rotating (i.e., fixed Cartesian coordinates), we can consider the reduced configuration space $\mathcal{Q} = \mathrm{SO}(3) \times \mathbb{S}^1$ for the continuous dynamics of single-support phase. We parameterize this space with the coordinate vector $q = (\psi, \varphi, \theta^T)^T \in \mathbb{T}^4$, where $\psi, \varphi \in \mathbb{S}^1$ are, respectively, the heading/yaw and roll/lean variables at the stance foot, and sagittal-plane vector $\theta = (\theta_{\mathrm{s}}, \theta_{\mathrm{ns}})^T \in \mathbb{T}^2$ contains the stance and swing leg pitch variables. This choice of coordinates will allow us to consider dynamical stability independent of the Cartesian workspace.

This simple biped has no hip link; therefore, each leg has identical single-support dynamics (i.e., gaits will consist of one step cycle). The system state is given by $x = (q^T, \dot{q}^T)^T$ in phase space $T\mathcal{Q}$, where vector $\dot{q} \in \mathbb{R}^4$ contains the joint velocities. Foot-ground impacts are the only discrete events, which are instantaneous and perfectly plastic; therefore, we define a simple hybrid dynamical system with one continuous phase

$$\begin{aligned} \dot{x} &= f(x) + g(x)u, && x \in D \backslash G \\ x^+ &= \Delta(x^-), && x^- \in G \end{aligned} \tag{1}$$

where $u \in \mathbb{R}^m$ is the control input vector for $m \leq 4$, domain $D \subset T\mathcal{Q}$ is the set of states with nonnegative swing foot height, switching set $G \subset D$ contains states where the swing foot height is zero and decreasing (a hyperplane in $T\mathcal{Q}$), and $\Delta : G \to D$ is the reset map modeling the discontinuous impact event. Details on these dynamics can be found in [12].

Given a state-feedback controller for input u, (1) becomes a closed-loop, time-invariant hybrid system that is solved by a curve $x(\cdot) : \mathbb{R}_+ \to T\mathcal{Q}$ called a *hybrid flow*. An appropriately designed controller will produce walking gaits that correspond to *periodic* hybrid flows such that $x(t) = x(t + T)$ for all $t \geq 0$ and some minimal $T > 0$ known as the time to impact between discrete events. When the image of a periodic flow in $T\mathcal{Q}$ is an isolated orbit, it is known as a *hybrid limit cycle*.

Hybrid limit cycles correspond to equilibria of the return map $P : G \to G$, which represents a hybrid system as a discrete system between impact events. This map sends state $x_i \in G$ ahead one step to $x_{i+1} =$

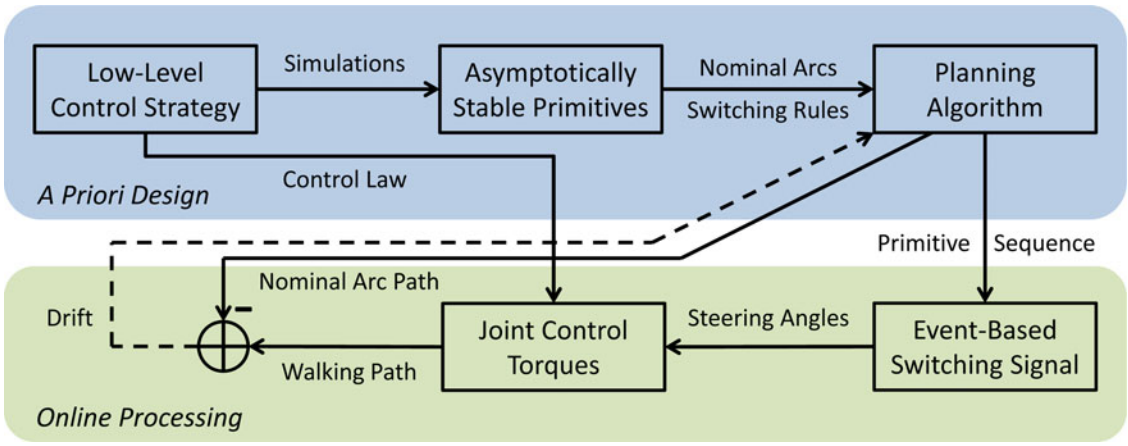

Fig. 2. Process flow diagram of planning framework. Dashed line represents feedback that would be needed for iterative planning to compensate for drift.

$P(x_i)$; therefore, a period-one hybrid limit cycle has a fixed point $x^* = P(x^*)$. We say that x^* is *stable* if for each $\epsilon > 0$, there exists a constant $\gamma > 0$ such that for all sequences $\{x_i\}$ with $|x_0 - x^*| \leq \gamma$, $|x_i - x^*| \leq \epsilon$ for all $i \geq 0$. A fixed point is LAS if it is stable *and* $|x_i - x^*| \to 0$ as $i \to \infty$.

We know that a hybrid limit cycle is LAS if its associated fixed point is LAS [1]. We verify LAS of x^* by computing the linearized map $\nabla_x P(x^*)$ in simulation [8]. This yields a discrete linear system that is asymptotically stable if the magnitudes of the eigenvalues of $\nabla_x P(x^*)$ are strictly less than one. The local stability region about fixed point x^*, which is known as the *basin of attraction*, is then

$$\mathrm{BoA}(x^*) = \left\{ x \in G \ \text{ s.t. } \lim_{i \to \infty} P^i(x) = x^* \right\}. \tag{2}$$

A walking gait corresponds to a LAS fixed point of return map P in local coordinates $x \in T\mathcal{Q}$. Turning gaits have a fixed change in heading s, resulting in a fixed point *modulo yaw*

$$x^*(s) + (s \quad 0_{1\times 7})^T = P_s(x^*(s)). \tag{3}$$

Straight-ahead gaits are then asymptotically stable about a zero steering angle. We will express fixed points as a function of steering angle s throughout the rest of this paper.

III. Asymptotically Stable Gait Primitives

We now use this construction to define asymptotically stable motion primitives. We will later see that this concept generalizes to more complex bipeds that admit LAS hybrid limit cycles, since hybrid mechanical systems can be defined as discrete systems using the method of Poincaré sections [1].

In the context of path planning, we must consider the robot's world coordinates in the generalized configuration space $\mathrm{SE}(3) \times \mathbb{S}^1$. For walking on a flat surface, we need only measure the SE(2) coordinates of stance foot position $p \in \mathbb{R}^2$ and heading $\psi \in \mathbb{S}^1$ (the first term in configuration vector q) at every step. The biped's extended state is then $x^{\mathrm{e}} = (p^T, x^T)^T \in \mathbb{R}^2 \times T\mathcal{Q}$ with extended return map P^{e}, which updates positions using forward kinematics.

Definition 1: Given a coordinate parameterization $h \in \mathrm{SE}(2)$, define the group action

$$\Phi_h(x^{\mathrm{e}}) = (h^T + (p^T, \psi), \varphi, \theta^T, \dot{q}^T)^T. \tag{4}$$

Extended map P^{e} is *equivariant* under SE(2) if for all $h \in \mathrm{SE}(2)$ and $x^{\mathrm{e}} \in \mathbb{R}^2 \times T\mathcal{Q}$, $\Phi_h \circ P^{\mathrm{e}}(x^{\mathrm{e}}) = P^{\mathrm{e}} \circ \Phi_h(x^{\mathrm{e}})$.

This symmetry property in the global coordinates is guaranteed on level ground when using a control law that is independent of heading ψ (based on SO(3)-invariance [17]). We can now formalize the notion of asymptotically stable motion primitives for 3-D walking through flat environments.

Definition 2: An *asymptotically stable gait primitive* with steering angle s is a pair $\mathcal{G}(s) = (P_s, x^*(s))$ such that (3) is satisfied and the extended map P_s^{e} is equivariant under SE(2).

The extended map of a gait primitive yields a fixed point in local coordinates and a walking arc in SE(2). Transient effects from gait switching (i.e., converging back and forth between differing orbits) prevent a fixed mapping from gaits to path arcs during a walking sequence, but each gait segment is approximated by a constant-curvature arc.

Definition 3: The *nominal walking arc* of primitive $\mathcal{G}(s)$ is the pair $\left(\delta p^T(s), s\right)^T \in \mathrm{SE}(2)$ with heading change s and position displacement $\delta p(s) \in \mathbb{R}^2$ from initial heading $\psi = 0$.

Walking arcs are composed with different orientations by rotating the nominal arc's coordinate frame to coincide with initial heading ψ, i.e., $R_\psi \delta p(s)$ where $R_\psi \in \mathrm{SO}(2)$ is the standard rotation matrix with respect to angle ψ.

The *basis* set $\mathcal{P}(s) = \{\mathcal{G}(0), \mathcal{G}(s), \mathcal{G}(-s)\}$ parameterized by steering angle s contains three primitives: straight ahead, clockwise (CW), and counterclockwise (CCW). This set grows a discrete tree of nominal arcs with branching factor three. If we derive *a priori* rules that ensure stable composition between primitives in a set $\mathcal{P}(s)$, we will have reduced a complicated kinodynamic planning problem in $\mathbb{R}^2 \times T\mathcal{Q}$ to a discrete search in SE(2). The planning algorithm can then be designed to output a sequence of steering angles parameterizing gait primitives (e.g., by preimage backchaining from the goal position [18]). The process flow diagram for this hierarchical planning framework is shown in Fig. 2.

In this construct, the output of the planner drives the event-based control $\sigma(\cdot)$ in the discrete switched system

$$x_{i+1}^{\mathrm{e}} = P_{\sigma(i)}^{\mathrm{e}}\left(x_i^{\mathrm{e}}\right) \tag{5}$$

where, at each impact event i, switching signal $\sigma : \mathbb{Z}_+ \to \{0, s, -s\}$ chooses a closed-loop system $P_{\sigma(i)}^{\mathrm{e}}$ parameterized by the steering angle of a primitive. We now derive constraints on angle s and signal σ that ensure stability of (5).

IV. Rules for Sequential Composition

We now present a switched system formulation of the funneling approach to controller composition [15], by which we derive our main technical contribution: an upper bound on the steering angle s parameterizing basis set $\mathcal{P}(s)$, and a lower bound on the switching frequency of σ in (5). These *a priori* rules will ensure stable composition of gait primitives for an n-DOF biped ($n = 4$ for our example), where we do not necessarily have a symbolic expression for the return map.

Definition 4: Step cycle i is represented by the pair $(x_{i-1}, \mathcal{G}_i)$, where $\mathcal{G}_i$ is the gait primitive employed after the $(i-1)$st impact event with impact state x_{i-1}. Step cycle i is said to be *switching* if $\mathcal{G}_i \neq \mathcal{G}_{i-1}$ and *stable* if $x_{i-1} \in \mathrm{BoA}(x_i^*)$, where x_i^* is the LAS fixed point of primitive $\mathcal{G}_i$.

Step cycle $i+1$ is then related to cycle i by $x_i = P_{\sigma(i)}(x_{i-1})$. Invariance of the basin of attraction implies that step cycle $i+1$ is stable if cycle i is stable and $\mathcal{G}_{i+1} = \mathcal{G}_i$. We derive the first rule for stable composition by exploiting a convergence property of continuously parameterized gaits.

Assumption 1: For every steering angle $s \in [-S, S]$ for some $S > 0$, there exists LAS fixed point $x^*(s)$ of P_s with corresponding $\mathrm{BoA}(x^*(s))$. Then, by definition, there exists a nonempty open ball of radius $r(s) > 0$ about $x^*(s)$ such that $\mathcal{B}(x^*(s), r(s)) \subset \mathrm{BoA}(x^*(s))$, where $x^*(s)$ and $r(s)$ are assumed continuous functions of s.

Property 1: Continuity of function $x^*(s)$ implies convergence to fixed point $x^*(0)$ in metric space $(\mathbb{R}^{2n}, d)$ as $s \to 0$, i.e., $\lim_{s\to 0} d(x^*(s), x^*(0)) = 0$ for Euclidean distance d.

Turning motion more closely resembles straight-ahead motion for smaller steering angles. We, then, can exploit overlap in neighboring basins of attraction to derive our first rule.

Rule 1: The absolute turning curvature $|s|$ of basis $\mathcal{P}(s)$ is bounded above by some $\tilde{S}$ satisfying Lemma 1.

Lemma 1: There exists a positive steering angle $\tilde{S} \leq S$ such that for all $s \in [-\tilde{S}, \tilde{S}]$

1) $x^*(0) \in \mathcal{B}(x^*(s), r(s)) \subset \mathrm{BoA}(x^*(s))$;
2) $x^*(s) \in \mathcal{B}(x^*(0), r(0)) \subset \mathrm{BoA}(x^*(0))$;
3) $x^*(-s) \in \mathcal{B}(x^*(s), r(s)) \subset \mathrm{BoA}(x^*(s))$.

Proof: [1.1] We first define minimal ball radius $\underline{r} := \min_{\hat{s}\in[-S,S]}(r(\hat{s}))$, positive by compactness of $[-S, S]$; therefore

$$\mathcal{B}(x^*(s), \underline{r}) \subset \mathcal{B}(x^*(s), r(s)) \subset \mathrm{BoA}(x^*(s))$$

for all $s \in [-S, S]$. Since $\underline{r} > 0$ and $\lim_{s\to 0} d(x^*(s), x^*(0)) = 0$, $\exists\ \tilde{S} \leq S$ such that $d(x^*(s), x^*(0)) < \underline{r}$ for all $s \in [-\tilde{S}, \tilde{S}]$. Then, $x^*(0) \in \mathcal{B}(x^*(s), \underline{r})$ for all $s \in [-\tilde{S}, \tilde{S}]$.

[1.2] Similarly, $x^*(s) \in \mathcal{B}(x^*(0), \underline{r})$ for all $s \in [-\tilde{S}, \tilde{S}]$.

[1.3] Recall $x^*(s) \to x^*(0)$ as $s \to 0$, which means that for each $\epsilon/2 > 0$, $\exists\ \delta > 0$ such that for all $s \in [-\delta, \delta]$, $d(x^*(s), x^*(0)) < \epsilon/2$. Then, the triangle inequality shows

$$d(x^*(s), x^*(-s)) \leq d(x^*(s), x^*(0)) + d(x^*(-s), x^*(0)) < \epsilon.$$

Hence, $\lim_{s\to 0} d(x^*(s), x^*(-s)) = 0$.

As in 1.1, $\exists\ \tilde{S}$ such that $d(x^*(s), x^*(-s)) < \underline{r}$ for all $s \in [-\tilde{S}, \tilde{S}]$. Then, $x^*(-s) \in \mathcal{B}(x^*(s), \underline{r})$ for all $s \in [-\tilde{S}, \tilde{S}]$.

Finally, we take the smallest $\tilde{S}$ from the three proofs. ■

Remark 1: If contained in open ball $\mathcal{B}(x^*(s), r(s))$, $x^*(0)$ cannot be on the boundary of $\mathrm{BoA}(x^*(s))$. Therefore, points sufficiently close to $x^*(0)$ are also contained in $\mathrm{BoA}(x^*(s))$. The same holds for the other claims in Lemma 1.

Although a converging trajectory never reaches a fixed point in finite time, the state will eventually be close enough for switching. If switching signal σ in (5) provides a sufficiently long *dwell time* for a primitive, the state will be funneled into the basins of attraction of the other primitives. Our second rule, therefore, constrains this signal to ensure stable composition.

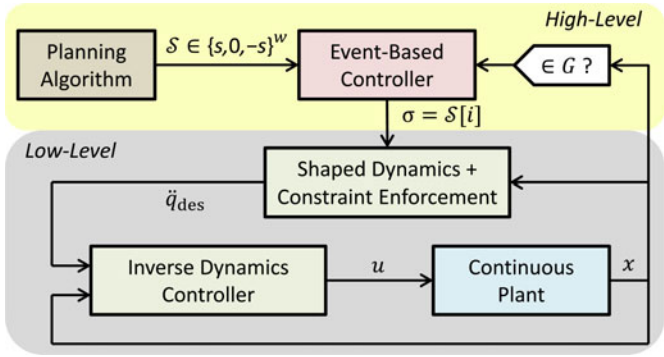

Fig. 3. Low-level and high-level control loops. Note that G is the switching set for ground strike, w is the number of primitives in a planned sequence, σ is the switching signal, and $\ddot{q}_{\mathrm{des}}$ are the closed-loop joint accelerations.

Rule 2: The switching signal σ of (5) has a minimum dwell time $N \geq 1$, i.e., $\sigma(i+j) = \sigma(i)$ for all $j \leq N$ and all i such that $\sigma(i-1) \neq \sigma(i)$, where N satisfies Theorem 1.

Theorem 1: For any $s \in [-\tilde{S}, \tilde{S}]$, there exists a minimal number of steps $N \geq 1$ such that for all integers $k \geq N$

1) if $x \in \mathcal{B}(x^*(0), r(0))$, then $P_0^k(x) \in \mathcal{B}(x^*(s), r(s))$;
2) if $x \in \mathcal{B}(x^*(s), r(s))$, then $P_s^k(x) \in \mathcal{B}(x^*(0), r(0))$;
3) if $x \in \mathcal{B}(x^*(s), r(s))$, then $P_s^k(x) \in \mathcal{B}(x^*(-s), r(-s))$.

Proof: We know from Lemma 1 and Remark 1 that for any pair $\hat{s}, \bar{s} \in [-\tilde{S}, \tilde{S}]^2$, $\exists\ \bar{r}(\hat{s}, \bar{s}) > 0$ (assumed continuous) such that $\mathcal{B}(x^*(\hat{s}), \bar{r}(\hat{s}, \bar{s})) \subset \mathcal{B}(x^*(\bar{s}), r(\bar{s}))$. By definition of LAS, for every $\epsilon > 0$ and $x \in \mathrm{BoA}(x^*(\hat{s}))$, $\exists\ N_{\epsilon,x}(\hat{s}) \geq 1$ such that for every $k \geq N_{\epsilon,x}(\hat{s})$, $d(P_{\hat{s}}^k(x), x^*(\hat{s})) < \epsilon$. Letting $\epsilon = \min_{\hat{s},\bar{s}\in[-\tilde{S},\tilde{S}]^2} \bar{r}(\hat{s}, \bar{s})$, positive by compactness of $[-\tilde{S}, \tilde{S}]^2$, $N = \max_{\hat{s}\in\{0,s,-s\}}\{\sup_{x\in\mathcal{B}(x^*(\hat{s}),r(\hat{s}))} N_{\epsilon,x}(\hat{s})\}$ is finite by completeness of $\mathbb{R}$ and satisfies claims 1–3. ■

Note that the minimum dwell time N is conservative, i.e., violating this rule does not necessarily imply instability. We may not always be able to explicitly compute the basins of attraction; therefore, in Section V, we propose a simulation-intensive heuristic to estimate the value of N. We will also numerically verify that the absolute steering angle is bounded above by $\tilde{S}$.

We have shown that the stability of a walking sequence is ensured *a priori* by two rules: an *upper bound on absolute curvature* and a *lower bound on dwell time*. A hierarchical controller (e.g., a finite-state machine) for signal σ can then piece together straight and curved segments such that the turns are not too sharp or the primitive switches too frequent. By considering LAS systems, this result is more broadly applicable than the dwell time derived for *globally exponentially* stable systems (a stronger form of LAS) in [14]. Our switching framework is also related to the aperiodic sense of stability considered in [2]. We now construct an example set of LAS gait primitives.

V. Compass-Gait Biped Example

We now apply this framework to the canonical example of the compass-gait biped. We will later demonstrate that the framework generalizes to more complex models that admit LAS gaits (e.g., [6], [13], [19], and [20]).

The first step is to choose a low-level controller that stabilizes a set of gaits for the hierarchical system in Fig. 3.

TABLE I
NOMINAL WALKING ARCS FOR COMPASS-GAIT BIPED

Primitive	Command	$\delta p_1(s)$ [m]	$\delta p_2(s)$ [m]	s [rad]
Straight	$\bar{\psi} = \psi$	0	0.534	0
CW	$\bar{\psi} = \psi + 0.32$	0.1733	0.5229	0.32
CCW	$\bar{\psi} = \psi - 0.32$	−0.1733	0.5229	−0.32

A. Choosing a Stabilizing Low-Level Controller

For simplicity, we assume full actuation ($m = n = 4$) in our compass-gait model, but we will consider an underactuated model in Section VI. The control input u is subject to actuator saturation, where $|u_j| \leq U^{\max}$ for all $j \in \{1, \ldots, 4\}$.

Reduction-based control exploits the existence of momentum conservation laws to decompose robot dynamics into lower dimensional control problems [11], [13]. These laws are nonholonomic constraints that can be controlled as in [13] and [20] to drive yaw toward desired heading $\bar{\psi}$ and stabilize lean about vertical $\bar{\varphi} = 0$. A geometric reduction with respect to these conservation laws defines a projection onto a reduced-order system corresponding to the decoupled sagittal plane (the $\hat{y}$-$\hat{z}$ plane in Fig. 1). Gaits are then constructed from passively stable periodic motions in the sagittal plane (e.g., [17]).

A feedback control law is designed for this purpose in [11], which inverts the plant and reinserts the original dynamics plus shaping and constraint enforcement terms (see [11] and [13] for details). This controller will interact with the planner as shown in Fig. 3, but we first must construct a set of gait primitives.

B. Constructing the Primitive Set

We assign common physical parameters from the literature to construct our primitive set: M = 10 kg, m = 5 kg, ℓ = 1 m, and $U^{\max}$ = 20 N·m. The closed-loop hybrid system yields straight-ahead walking on flat ground by setting $\bar{\psi} = 0$ (without loss of generality) to find the fixed point $x^*(0)$ as in [12]. We numerically verify LAS of this straight-ahead gait by linearizing the associated Poincaré map P_0. This defines the straight-ahead gait primitive $\mathcal{G}(0) = (P_0, x^*(0))$, which has a periodic step length of 0.534 m and speed of 0.727 m/s.

We create turning gaits by steering with a constant angle s between steps, where the event-based controller in (5) increments desired yaw $\bar{\psi}$ by s at each impact event [12]. We want to show that for sufficiently small s, trajectories of the hybrid system converge to a period-one orbit corresponding to an LAS fixed point (modulo yaw) of P_s. We can then define CW-turning and CCW-turning gait primitives $\mathcal{G}(s)$ and $\mathcal{G}(-s)$, which have mirroring orbits in the yaw/lean coordinates.

Initialized at $x^*(0)$, we observe convergence to a fixed point $x^*(s)$ for any choice of $s \in [-S, S]$, $S = 0.492$. We densely sample steering values in $[-S, S]$, find the fixed point for each sample, and confirm LAS as numerical evidence of Assumption 1 and Property 1. Input-to-state stability provides that trajectories will remain nearby for steering values between sufficiently dense samples (arguably with LAS fixed points). The position displacements for the nominal walking arc associated with each steering angle are given in Fig. 4.

Although it is difficult to find the exact steering bound $\tilde{S}$ for Rule 1, we can easily verify the conditions of Lemma 1 for some s by checking convergence from all fixed points of basis set $\mathcal{P}(s)$. We confirm that Rule 1 is satisfied for $\tilde{s} = 0.32$ (i.e., $\tilde{s} \leq \tilde{S}$). The nominal walking arcs of basis set $\mathcal{P}(\tilde{s})$ are given in Table I (see [12] for the fixed points). We also verify that these simulated gaits do not violate unilateral ground contact constraints by calculating the ground reaction forces as in [13].

We now must numerically derive the minimum dwell time of Rule 2 for this basis set of primitives.

C. Computing the Switching Bound

The overlapping region between basins of attraction influences the minimum dwell time N for Theorem 1. If the biped's transient state leaves this safe region, an unstable switching scenario becomes possible. In particular, high-frequency switching may not provide sufficient time for a gait to attenuate transients. Eventually, the impact-event state from one gait primitive may be outside the basin of attraction of the next.

We attempt to deduce N for $\mathcal{P}(\tilde{s})$ by exhaustively testing gait switching scenarios with a "random walk," picking a gait primitive every step from a uniform random distribution. We observe occasional falls after dozens of steps, implying that $N > 1$. We next allow switching every other step and are unable to produce falls after several lengthy simulations (1000+ steps), suggesting that minimum dwell time $N = 2$.

This simulation-intensive procedure explores a lower dimensional discrete space of sequences rather than the full continuous state space, which allows application to high-dimensional bipeds. The resulting estimate is not rigorous, but we have shown that falling scenarios are rare for the states commonly encountered during walking. Emerging work on transverse dynamics and sum-of-squares verification to estimate basins of attraction of hybrid limit cycles [21] may prove essential for rigorous bounds on dwell time [14].

These simulations provide evidence that the overlapping attractive region of the primitive set is large, due to the close proximity of the fixed points, as well as the large sizes of the associated basins of attraction. Hence, this primitive set is capable of building a large class of stable walking paths, enabling planning through workspaces (animated on the right side of Fig. 4).

VI. PATH PLANNING APPLICATIONS

The gait primitive framework (see Fig. 2) provides a layer of abstraction above the low-level control and stability of a walking mechanism to enable motion planning by switching between prestabilized gaits. We can compose these separate primitives in discrete pieces to generate trajectories that simultaneously perform obstacle avoidance and direct the robot to a goal region in the workspace. In this section, we present one possible approach to planning based on gait primitives as a proof of concept. Note, however, that the development of this paper opens the possibility of a wide variety of planning algorithms being used in real robot systems.

We begin with a basis primitive set, which corresponds to a discrete subset of the continuous range of steering angles available to the biped. The set of possible paths (concatenations of motion primitives) can then be characterized by a tree data structure with branching factor equal to the cardinality of the primitive set. The number of paths encoded in this tree expands exponentially as the number d of concatenated primitives in a path grows. Thus, the tree will represent $O(3^d)$ paths composed of nominal walking arcs. If d is large (the path length to be walked is long) and we wish to choose a path based on certain criteria, i.e., collision free, reaches the goal, and minimizes a cost function, we will need to heuristically bias the exploration of the search tree. This is a well-studied problem [22]–[24], and in particular, the A* graph search algorithm is frequently applied to humanoid robots, e.g., [10] and [25]. We will use a variant of [25] to plan our walking paths.

We define initial world configuration $c_0 \in \mathrm{SE}(2)$ and goal region $F \subset \mathrm{SE}(2)$ so that any stable walking sequence ending at a world configuration $c_w \in F$ after some number of steps w is considered admissible. The planner outputs a steering sequence $\mathcal{S}_w \in \{0, s, -s\}^w$ corresponding to the gait primitive for each step in the walking path. This sequence is designed to produce a trajectory in system (5) that is collision free and terminates in the goal region, while minimizing a

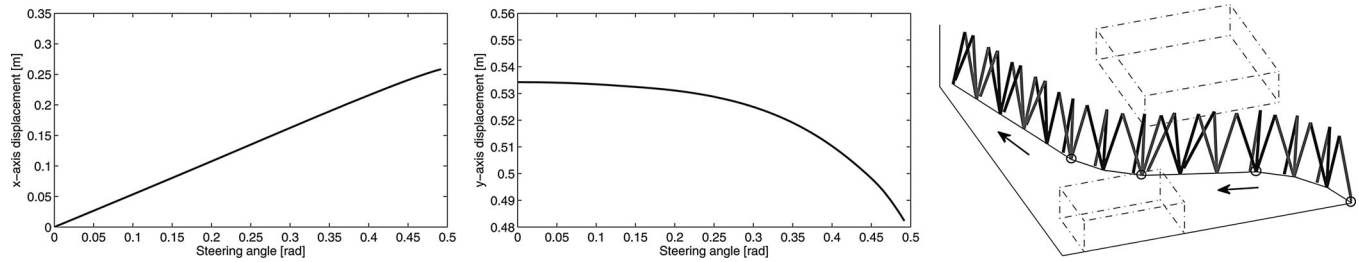

Fig. 4. Evolution of (left) $\hat{x}$-axis and (right) $\hat{y}$-axis displacements over steering angle $s \in [0, 0.492]$. (Right) Animation of an example planned walking sequence. The sequence of primitives is (CCW, CCW, CCW, S, S, S, CW, CW, S, S, S, S, S), where switching steps are indicated by circles at impact events.

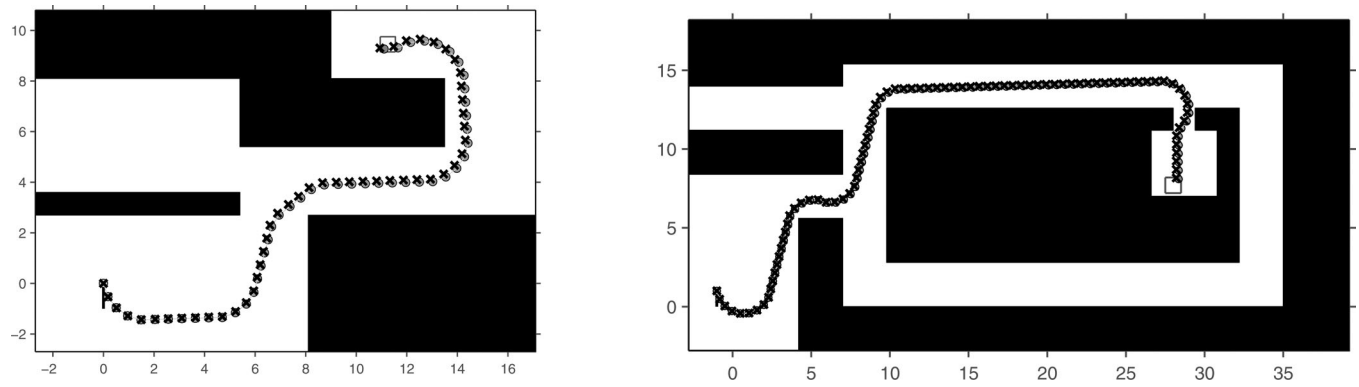

Fig. 5. Two planned walking environments with basis set $\mathcal{P}(\tilde{s})$, $\tilde{s} = 0.32$. Planned steps are indicated by gray circles and simulated steps by black X's. Initial orientation is shown by a black line from the starting position. Maximum, mean, and final drift values are, respectively, (left) 0.197, 0.107, and 0.169 m and (right) 0.168, 0.105, and 0.168 m. Supplementary downloadable videos are available for these planned walking cases.

scalarized objective function $\mathcal{C}[\mathcal{S}_w]$ that penalizes nominal path length and number of gait switches (according to weight factor α)

$$\mathcal{C}[\mathcal{S}_w] = \sum_{i=1}^{w} \text{norm}(\delta p(\mathcal{S}_w(i))) + \alpha \mathbb{1}\{\mathcal{S}_w(i) \neq \mathcal{S}_w(i-1)\}.$$

The planner begins by performing a workspace decomposition that bounds obstacles with safety regions and decomposes the free space into a set of convex cells. We use the shortest path on the workspace skeleton[1] to identify the path homotopy class[2] we will explore to find our path composed of motion primitives. This heuristic works well in practice for reducing the number of paths to be explored without removing desirable paths [25]. Our second complexity-reducing approximation is a branch and bound style of tree search, where we plan optimal sequences of motion primitives between subgoal regions in the configuration space. We identify these subgoals by finding intersections between workspace curves corresponding to the projection of paths belonging to our selected homotopy class and boundaries of the workspace decomposition.

We employ the A* Algorithm to compute optimal paths between subgoals. This algorithm expands the search tree by choosing nodes from a priority queue that is sorted by the *cost-to-come*, a partial computation of $\mathcal{C}$ (on the segment of the primitive sequence explored thus far), plus the estimated *cost-to-go*. The true cost-to-go from a node, i.e., the minimal cost to reach the goal set from the configuration of that node, is not known until the algorithm completes; therefore, it is approximated with a heuristic function that lower bounds the true cost-to-go. For this, we use the Euclidean distance between workspace projections of the robot's configuration at the node and the closest point in the next subgoal region. Sequences of motion primitives that violate dwell-time constraints or likely cause obstacle collisions are pruned during the process of node expansion. When A* terminates, we have a path plan from one subgoal region to the next. We can then start a new search from the terminal configuration of this path to the next subgoal region. The final subgoal region is identical to the goal region, by which the plan generation is completed.

A. Compass-Gait Biped Results

We use the primitive basis set $\mathcal{P}(\tilde{s})$ of Table I with $\tilde{s} = 0.32$. Setting weight factor $\alpha = 0.6$, the planner takes seconds to produce the nominal paths shown in gray in the example environments in Fig. 5. The compass-gait biped is then simulated with the corresponding sequence of primitives, resulting in a walking path (shown in black) that traces the preplanned path into the goal region with only minor drift. In both cases, the average and final errors from planned step placements are, respectively, 20% and 32% of one step length.

Recall that the biped does not explicitly track this planned path. The nominal walking arcs associated with the open-loop primitive sequence accurately predict the simulated walking path. This is noteworthy given the transient effects after each switching step. Hundreds of randomly generated paths show that final drift is more strongly correlated with the number of switches than steps (determination coefficients of 0.64

[1]The workspace skeleton is a deformation retract of the free workspace, which is implemented as a discrete approximation of the generalized Voronoi diagram.

[2]Two paths that are homotopic to one another are identical after a homotopic transformation corresponding to a deformation retract [23].

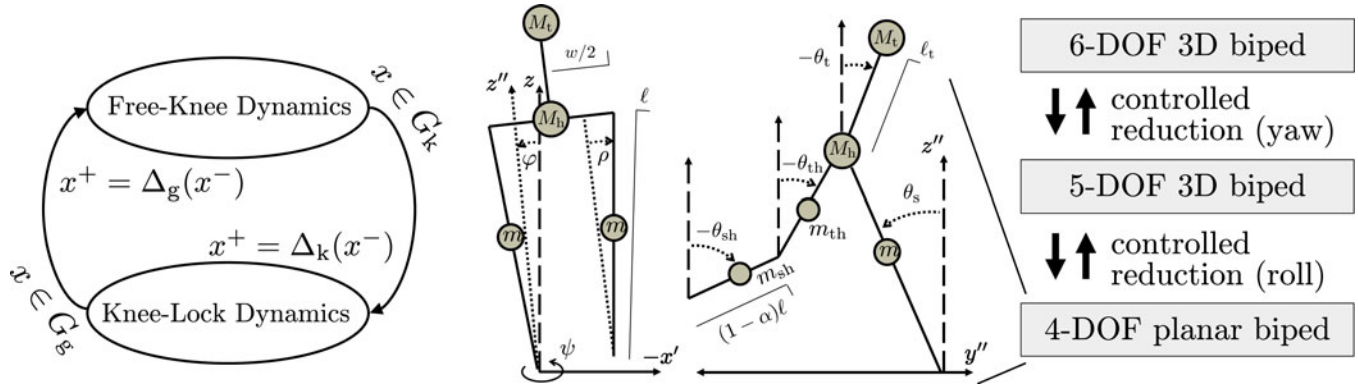

Fig. 6. Diagrams of the (left) five-link 3-D biped's hybrid system, (middle) frontal and sagittal planes, and (right) controlled reduction. The control strategy decouples the dynamics of the sagittal plane by reducing the yaw DOF of the transverse plane and the roll/lean DOF of the frontal plane.

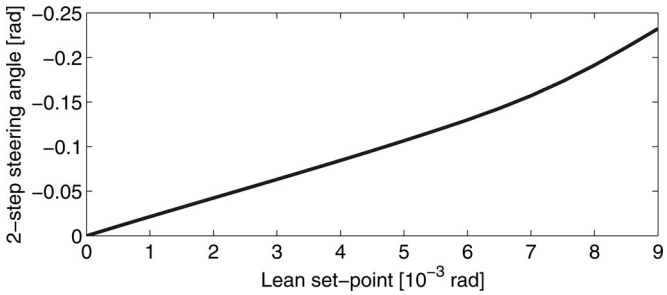

Fig. 7. Five-link biped. Two-step steering angle of steady-state turning gait against lean set point $\bar{\varphi}$ of the inner leg's stance phase. This curve is an odd function of the lean set point, i.e., negating the $\hat{x}$-axis negates the $\hat{y}$-axis.

versus 0.28). Occasional replanning, as suggested in Fig. 2, can easily compensate for drift accumulation after many switches/steps.

B. Five-Link Biped Results

This planning framework can be applied to a large class of bipedal walkers that admit hybrid limit cycles satisfying Property 1. Model complexity and underactuation only challenges the low-level control design. We now demonstrate how the planner generalizes to more complex models by considering the underactuated five-link 3-D biped of [19] shown in Fig. 6.

Given the same foot contact assumptions for the compass-gait biped, the hybrid system of the five-link biped has two distinct phases during single support: knee swing with six DOFs and knee lock with five DOFs. We assume that both knee-strike and ground-strike impact events (respectively triggered by sets G_k and G_g) are instantaneous and perfectly plastic, resulting in transitions between the six and five DOF dynamics according to the left side of Fig. 6. The knee of the stance leg remains locked through the entire single-support cycle. The yaw DOF at the ankle is unactuated but subject to viscous damping from friction (which stabilizes this motion [13]). The other DOFs including ankle lean and pitch are actuated ($m = n - 1$) with a torque bound of 40 N·m. We adopt the underactuated formulation of reduction-based control from [13] to construct a set of two-step gait primitives for this 35-kg biped, where heading is controlled by leaning into turns.

We characterize the state evolution over a two-step gait cycle by twice composing the return map $P : G_g \to G_g$. The Poincaré map P^2 gives us fixed points as before, reducing this complex hybrid system to the simple construction of Sections III and IV. Due to the unactuated yaw DOF, the steering angle $s = s(\bar{\varphi})$ is now a function of the lean set point. Fig. 7 shows that this (odd) function is continuous and one to one, allowing satisfaction of Property 1 as before.

TABLE II
NOMINAL WALKING ARCS FOR FIVE-LINK BIPED

Primitive	Command	δp_1 [m]	δp_2 [m]	s [rad]
Straight	$\bar{\varphi} = 0$	0	1.1970	0
CW	$\bar{\varphi} = -0.009$	0.1962	1.1751	0.1968
CCW	$\bar{\varphi} = 0.009$	−0.1962	1.1751	−0.1968

The basis set of primitives $\mathcal{P}(s(\bar{\varphi}))$ that are derived from $\bar{\varphi} = 0.009$ is given in Table II. These primitives satisfy Lemmas 1.1 and 1.2 and Theorems 1.1 and 1.2; therefore, switches are possible between turning and straight-ahead gaits but not necessarily between opposing (CW/CCW) turning gaits. We estimate the minimum dwell time for these relaxed conditions following the procedure in Section V-C and find that switching between straight ahead and turning is allowed every gait cycle ($N = 1$). Integrating instantaneous power to compute the work done per unit weight per unit distance, we find that the mechanical cost of transport for each primitive is small at 0.037 and similar to passive dynamic walkers such as the Cornell biped at 0.055 [26].

The only modification needed in the previously described planning algorithm is that branches corresponding to switches between CW/CCW are also pruned during node expansion. We expect greater transient drift from preplanned walking paths due to this model's lack of direct steering control; therefore, we expand the safety boundaries around obstacles and further penalize switches with $\alpha = 1$. Before simulating the path output by the planner, we delete the first two primitives (and twice repeat the last) in the sequence so that the biped employs each gait primitive two cycles early. This causes leaning ahead of planned turns to further reduce drift from the desired path.

Fig. 8 shows the planned and simulated paths of the (enlarged) first example environment. The drift from the desired destination is 2.59 m after an open-loop sequence of 104 steps, which can be improved with an iterative planning algorithm. The fact that our high-level framework is applicable to complex biped models without direct control over steering is a testament to the significance of the approach. We have enabled dynamic walking through workspaces for 3-D robots that have similar energetic efficiency to passive dynamic walkers.

VII. CONCLUSION

We have reduced a complicated feedback motion planning problem in a high-dimensional state space to a much simpler discrete path planning problem with a low-dimensional characterization of the robot's

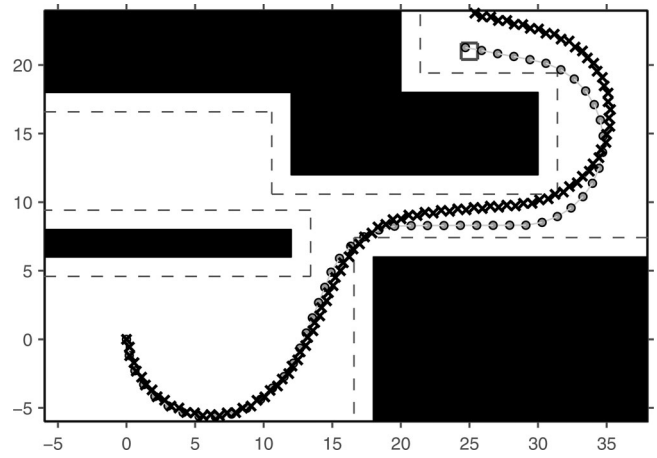

Fig. 8 Five-link biped. Planned walking with primitive set $\mathcal{P}(\bar{\varphi})$, $\bar{\varphi} = 0.009$. Nominal primitive arcs are connected by gray circles (representing the second step of a gait cycle) and simulated steps are indicated by black X's. Obstacle safety region of planner delineated by dashed boundaries. The drift from the desired destination is 2.59 m after an open-loop sequence of 104 steps.

configuration. This allows decomposed planning of asymptotically stable bipedal walking using search tools developed for ZMP walking [9], [10], [27], [28].

Our planning framework can potentially be used with any form of locomotion based on asymptotically stable gaits (e.g., walking [1], [6], [13], [20], brachiating [4], climbing [5], or running [1], [29]). Each gait primitive is characterized by a stabilizing controller and a fixed point, where the associated hybrid limit cycle is LAS in the closed-loop robot dynamics. Walking motion is not prescribed by full-state trajectories or subjected to postural ZMP constraints, yet we have stability over a large class of paths composed of gait primitives.

In order to reach specific goal configurations, future work might generalize this framework to allow primitive switching within the full continuous range of available steering angles. Gait primitives and their stability rules might also be precomputed using the feedback motion planning method of randomized linear quadratic regulator trees [30] with sum-of-squares programming [21]. Practical implementations of the gait primitive framework could integrate a suite of other feedback motion planning tools, such as step-level planning over rough terrain [31]–[33] and time scaling for variable walking speeds [34].

Asymptotically stable walking has been experimentally demonstrated on planar bipeds (e.g., [1]–[3]), and 3-D results will soon be possible with advances in controller and hardware design. The yaw DOF in our five-link biped can be controlled passively with viscous damping [13], allowing more feasible 2-DOF ankle actuation for lean and pitch. Preliminary work has implemented controlled reduction on a 16-DOF Sarcos humanoid model to achieve stable balancing [20] and on the NAO robot for experimental straight-ahead walking [35]. Similar advances will enable humanoid robots to employ our asymptotically stable motion planning framework.

References

[1] E. R. Westervelt, J. W. Grizzle, C. Chevallereau, J. H. Choi, and B. Morris, *Feedback Control of Dynamic Bipedal Robot Locomotion*. Boca Raton, FL: CRC, 2007.

[2] T. Yang, E. R. Westervelt, A. Serrani, and J. Schmiedeler, "A framework for the control of stable aperiodic walking in underactuated planar bipeds," *Auton. Robots*, vol. 27, no. 3, pp. 277–290, 2009.

[3] K. Sreenath, H. W. Park, I. Poulakakis, and J. W. Grizzle, "A compliant hybrid zero dynamics controller for stable, efficient and fast bipedal walking on MABEL," *Int. J. Robot. Res.*, vol. 30, no. 9, pp. 1170–1193, 2011.

[4] N. Rosa, A. Barber, R. D. Gregg, and K. M. Lynch, "Stable open-loop brachiation on a vertical wall," in *Proc. IEEE Int. Conf. Robot. Autom.*, St. Paul, MN, May 2012, pp. 1193–1199.

[5] A. Degani, S. Feng, H. Brown, K. Lynch, H. Choset, and M. Mason, "The Parkourbot—A dynamic bowleg climbing robot," in *Proc. IEEE Int. Conf. Robot. Autom.*, Shanghai, China, May 2011, pp. 795–801.

[6] C. Chevallereau, J. W. Grizzle, and C. L. Shih, "Steering of a 3D bipedal robot with an underactuated ankle," in *Proc. IEEE Int. Conf. Intell. Robots Syst.*, Taipei, Taiwan, Oct. 2010, pp. 1242–1247.

[7] M. Vukobratovic and B. Borovac, "Zero-moment point—thirty years of its life," *Int. J. Humanoid Robot.*, vol. 1, no. 1, pp. 157–174, 2004.

[8] A. Goswami, B. Thuilot, and B. Espiau, "A study of the passive gait of a compass-like biped robot: Symmetry and chaos," *Int. J. Robot. Res.*, vol. 17, no. 12, pp. 1282–1301, 1998.

[9] K. Hauser, T. Bretl, J.-C. Latombe, K. Harada, and B. Wilcox, "Motion planning for legged robots on varied terrain," *Int. J. Robot. Res.*, vol. 27, no. 11–12, pp. 1325–1349, 2008.

[10] J. J. Kuffner Jr., S. Kagami, K. Nishiwaki, M. Inaba, and H. Inoue, "Dynamically-stable motion planning for humanoid robots," *Auton. Robots*, vol. 1, no. 12, pp. 105–118, 2002.

[11] R. D. Gregg and M. W. Spong, "Reduction-based control of three-dimensional bipedal walking robots," *Int. J. Robot. Res.*, vol. 26, no. 6, pp. 680–702, 2010.

[12] R. D. Gregg and M. W. Spong, "Bringing the compass-gait bipedal walker to three dimensions," in *Proc. IEEE Int. Conf. Intell. Robots Syst.*, St. Louis, MO, Oct. 2009, pp. 4469–4474.

[13] R. D. Gregg, "Controlled geometric reduction of a five-link 3D biped with unactuated yaw," in *Proc. IEEE Conf. Decision Control*, Orlando, FL, Dec. 2011, pp. 669–674.

[14] T. Alpcan and T. Basar, "A stability result for switched systems with multiple equilibria," *Dyn. Continuous, Discr. Impulsive Syst.*, vol. 17, pp. 949–958, 2010.

[15] R. Burridge, A. Rizzi, and D. Koditschek, "Sequential composition of dynamically dexterous robot behaviors," *Int. J. Robot. Res.*, vol. 18, no. 6, pp. 534–555, 1999.

[16] R. D. Gregg, T. W. Bretl, and M. W. Spong, "Asymptotically stable gait primitives for planning dynamic bipedal locomotion in three dimensions," in *Proc. IEEE Int. Conf. Robot. Autom.*, Anchorage, AK, May 2010, pp. 1695–1702.

[17] M. W. Spong and F. Bullo, "Controlled symmetries and passive walking," *IEEE Trans. Autom. Control*, vol. 50, no. 7, pp. 1025–1031, Jul. 2005.

[18] T. Lozano-Pérez, M. Mason, and R. Taylor, "Automatic synthesis of fine-motion strategies for robots," *Int. J. Robot. Res.*, vol. 3, no. 1, pp. 3–23, 1984.

[19] R. D. Gregg, Y. Dhaher, A. Degani, and K. M. Lynch, "On the mechanics of functional asymmetry in bipedal walking," *IEEE Trans. Biomed. Eng.*, vol. 59, no. 5, pp. 1310–1318, May 2012.

[20] R. D. Gregg, L. Righetti, J. Buchli, and S. Schaal, "Constrained accelerations for controlled geometric reduction: Sagittal-plane decoupling in bipedal locomotion," in *Proc. IEEE Int. Conf. Humanoid Robots*, Nashville, TN, Dec. 2010, pp. 1–7.

[21] I. R. Manchester, "Transverse dynamics and regions of stability for nonlinear hybrid limit cycles," presented at the Int. Fed. Autom. Control Conf., Milano, Italy, 2011.

[22] J. Barraquand and J.-C. Latombe, "Nonholonomic multibody mobile robots: Controllability and motion planning in the presence of obstacles," *Algorithmica*, vol. 10, no. 2, pp. 121–155, 1993.

[23] H. M. Choset, K. M. Lynch, S. Hutchinson, G. Kantor, W. Burgard, L. E. Kavraki, and S. Thrun, *Principles of Robot Motion*. Cambridge, MA: MIT Press, 2005.

[24] S. M. LaValle, *Planning Algorithms*. New York: Cambridge Univ. Press, 2006.

[25] S. Candido, Y. T. Kim, and S. Hutchinson, "An improved hierarchical motion planner for humanoid robots," in *Proc. IEEE Int. Conf. Humanoid Robots*, Daejeon, Korea, Dec. 2008, pp. 654–661.

[26] S. H. Collins and A. Ruina, "A bipedal walking robot with efficient and human-like gait," in *Proc. IEEE Int. Conf. Robot. Autom.*, Barcelona, Spain, Apr. 2005, pp. 1983–1988.

[27] E. Yoshida, C. Esteves, I. Belousov, J.-P. Laumond, T. Sakaguchi, and K. Yokoi, "Planning 3-D collision-free dynamic robotic motion through iterative reshaping," *IEEE Trans. Robot.*, vol. 24, no. 5, pp. 1186–1198, Oct. 2008.

[28] S. Dalibard, A. E. Khoury, F. Lamiraux, M. Taix, and J. P. Laumond, "Small-space controllability of a walking humanoid robot," in *Proc. IEEE Int. Conf. Humanoid Robots*, Oct. 2011, pp. 739–744.
[29] J. Shill, B. Miller, J. Schmitt, and J. E. Clark, "Design of a dynamically stable horizontal plane runner," in *Proc. IEEE Int. Conf. Robot. Autom.*, Anchorage, AK, May 2010, pp. 4749–4754.
[30] R. Tedrake, I. R. Manchester, M. M. Tobenkin, and J. W. Roberts, "LQR-Trees: Feedback motion planning via sums-of-squares verification," *Int. J. Robot. Res.*, vol. 29, no. 8, pp. 1038–1052, 2010.
[31] F. Iida and R. Tedrake, "Minimalistic control of biped walking in rough terrain," *Auton. Robots*, vol. 28, no. 3, pp. 355–368, 2010.
[32] I. R. Manchester, U. Mettin, F. Iida, and R. Tedrake, "Stable dynamic walking over uneven terrain," *Int. J. Robot. Res.*, vol. 30, no. 3, pp. 265–279, 2011.
[33] S. Ramamoorthy and B. Kuipers, "Trajectory generation for dynamic bipedal walking through qualitative model based manifold learning," in *Proc. IEEE Int. Conf. Robot. Autom.*, Pasadena, CA, May 2008, pp. 359–366.
[34] J. K. Holm, D. Lee, and M. W. Spong, "Time-scaling trajectories of passive-dynamic bipedal robots," in *Proc. IEEE Int. Conf. Robot. Autom.*, Roma, Italy, Apr. 2007, pp. 3603–3608.
[35] R. Sinnet and A. D. Ames, "Bio-inspired feedback control of three-dimensional humanlike bipedal robots," *J. Robot. Mechatronics*, vol. 24, no. 4, Aug. 2012.

Active Vision During Coordinated Head/Eye Movements in a Humanoid Robot

Xutao Kuang, Mark Gibson, Bertram E. Shi, and Michele Rucci

***Abstract*—While looking at a point in the scene, humans continually perform smooth eye movements to compensate for involuntary head rotations. Since the optical nodal points of the eyes do not lie on the head rotation axes, this behavior yields useful 3-D information in the form of visual parallax. Here, we describe the replication of this behavior in a humanoid robot. We have developed a method for egocentric distance estimation based on the parallax that emerges during compensatory head/eye movements. This method was tested in a robotic platform equipped with an anthropomorphic neck and two binocular pan-tilt units specifically designed to reproduce the visual input signals experienced by humans. We show that this approach yields accurate and robust estimation of egocentric distance within the space nearby the agent. These results provide a further demonstration of how behavior facilitates the solution of complex perceptual problems.**

***Index Terms*—Active perception, behavior-based systems, biologically inspired robots, humanoid robots, 3-D vision.**

I. Introduction

Autonomous robots often need accurate estimation of the distance of objects and surfaces in the nearby space. Use of visual information would be ideally suited for this task. However, artificial 3-D vision systems remain highly sensitive to changes in their operating conditions, thus, seriously limiting the overall degree of robustness of the agent. Nature has faced a similar problem in the development of self-sufficient organisms. While stereopsis has become the predominant 3-D vision technique in robotics [1], [2], depth perception in humans and other species is an extremely robust process which relies on the analysis of multiple visual cues.

A highly informative cue used by many species is motion parallax, the displacement in the retinal position of the projection of an object as an agent moves through the environment [3]. In robotics, most of the work on this cue (a field known as depth from motion) has concentrated on large relocations of mobile platforms [4]–[12]. However, there is overwhelming evidence from biology that 3-D vision systems also benefit from the parallax resulting from more subtle movements, such as head and eye movements [13]–[16]. Before striking a prey, various types of insects, including the grasshopper and the mantis, perform peculiar peering head movements [17], which have been shown to contribute to perceptual judgments of distance. Similar exploratory head movements have also been observed in birds [18] and primates [19]. In humans, motion parallax resulting from head motion is used in various ways, including the control of body sway [20], and presentation on a 2-D display of stimuli that move by different amounts synchronously with the head induces a vivid 3-D percept [3].

Motion parallax resulting from head and eye movements is complementary to the stereo disparity cue usually considered by active binocular vision systems. By working simultaneously on each camera, this cue would increase the robustness of a binocular system, as it would continue to provide information even in the event of failure of one of the cameras. It would also enlarge the 3-D field of view, as it enables extraction of depth information in the regions that lack binocular overlap. Furthermore, it provides a controllable tradeoff between depth accuracy and computational complexity. In a stereo system, the disparity range over which to search for corresponding points is primarily determined by the distance between the two cameras (a fixed parameter, for a given robot), whereas with parallax, the search range varies with the amount of motion performed.

Here, we examine the 3-D information provided by motion parallax in an anthropomorphic robotic system that replicates the coordinated head/eye movements by which humans maintain normal fixation. Past work has considered only head or eye movements in isolation. For example, a recent study emulated the head movements of insects and birds for distance estimation [21]. Previous work from our group has shown that replication of human eye movements yields accurate estimation of egocentric distance within a range of nearby distances [22], [23]. However, no previous study has examined the impact of mutually compensatory head and eye movements similar to those continually performed by humans under natural viewing conditions. These movements maintain the attended objects at the center of the visual field, while providing reliable parallax.

The remainder of this paper is organized as follows. Section II describes a method for distance estimation based on the motion parallax caused by joint head and eye rotations. Section III examines its performance and robustness by means of computer simulations. Sections IV and V detail the results of robotic experiments. Section VI concludes this paper.

II. Distance Estimation Based on Head/Eye Motion Parallax

During fixation, humans use small head and eye movements to maintain the target within the fovea, the region on the retina with highest resolution. Since the focal nodal points of the eyes do not lie on the

Manuscript received January 27, 2012; accepted June 1, 2012. Date of publication July 17, 2012; date of current version December 3, 2012. This work was supported by the National Science Foundation under Grant CCF-0726901 and Grant BCS-1127216. This paper was recommended for publication by Associate Editor J. A. Castellanos and Editor D. Fox upon evaluation of the reviewers' comments.

X. Kuang, M. Gibson, and M. Rucci are with the Department of Psychology, Boston University, Boston, MA 02215 USA (e-mail: xtk@bu.edu; mggibson@bu.edu; mrucci@bu.edu).

B. E. Shi is with the Department of Electronic and Computer Engineering, The Hong Kong University of Science and Technology, Kowloon, Hong Kong (e-mail: eebert@ee.ust.hk).

Digital Object Identifier 10.1109/TRO.2012.2204513